10(2013) 953 – 980


# Material and geometric nonlinear analysis of reinforced concrete frame structures considering the influence of shear strength complementary mechanisms

**Abstract**

A mechanical model for the analysis of reinforced concrete frame structures based on the Finite Element Method (FEM) is proposed in this paper. The nonlinear behavior of the steel and concrete is modeled by plasticity and damage models, respectively. In addition, geometric nonlinearity is considered by an updated lagrangian description, which allows writing the structure equilibrium in the last balanced configuration. To improve the modeling of the shear influence, concrete strength complementary mechanisms, such as aggregate interlock and dowel action are taken into account. A simplified model to compute the shear reinforcement contribution is also proposed. The main advantage of such a model is that it incorporates all these effects in a one-dimensional finite element formulation. Two tests were performed to compare the provided numerical solutions with experimental results and other one- and bi-dimensional numerical approaches. The tests have shown a good agreement between the proposed model and experimental results, especially when the shear complementary mechanisms are considered. All the numerical applications were performed considering monotonic loading.

**Keywords**

dowel action, aggregate interlock, damage, plasticity, reinforced concrete, geometric nonlinearity, shear reinforcement, monotonic loading.

**C.G. Nogueira*, W.S. Venturini and H.B. Coda**

University of São Paulo, São Carlos Engineering School, Av. Trabalhador Sãocarlense 400 – São Carlos, São Paulo, Brazil

Received 14 May 2012
In revised form 07 Feb 2013

*Author email: gorlanog@sc.usp.br

## 1 INTRODUCTION

Nowadays, the search for mathematical models that accurately represent the mechanical behavior of reinforced concrete elements is still intense. Several phenomena present in the reinforced concrete make it a very complex and difficult material to model. Although complex models are usually more representative of the real behavior of the materials, they may cause more numerical problems and require more time of processing. A great challenge today is the development of more accurate mod-

els with simple formulations and easy accessibility to computational codes already established. However, some barriers must be overcome, as, for example, the proper representation of the reinforced concrete behavior with respect to shear strength and all the complementary mechanisms.

The FEM has been successfully used in the modeling of reinforced concrete structures, although its classical formulation does not consider the shear influence and its strength complementary mechanisms. Among these mechanisms, the aggregate interlock, dowel action, bond-slip behavior between steel and surrounding concrete and tension stiffening can be cited. The first works in this area, such as those by Krefeld and Thurston [19], Dei Poli et al. [9], Gergely [14], Dulacska [10], Jimenez et al. [18], Walraven [33], Laible et al. [21], Bazant and Gambarova [3] and Millard and Johnson [25] were performed to identify these mechanisms and discover how they interact with each other during the loading process along the reinforced concrete members. Later, researches were directed to the development of mathematical models to represent these phenomena and their implementation in FEM formulations. Most of those developments were considered in 2D FEM formulations with elastoplastic constitutive laws for concrete and steel. In these formulations, the reinforcement bars are taken into account by 1D finite elements embedded in the concrete plane elements and distributed along the longitudinal and transversal directions, as shown in the works of Bhatt and Kader [6], Martín-Perez and Pantazopoulou [23], He and Kwan [16], El-Ariss [11], Oliver et al. [27], Frantzeskakis and Theillout [13], Soltani et al. [31], Maitra et al. [22], Belletti et al. [5], Ince et al. [17] and Nogueira [26].

This paper presents a mechanical model based on one-dimensional finite element method taking into account the aggregate interlock, dowel action and shear reinforcement contributions in the reinforcement concrete member's strength. These phenomena were adapted to a plane frame finite element (1D) coupled with a damage model for concrete and an elastoplastic model for the reinforcements. Each mechanism was incorporated in a nonlinear finite element computational code already developed. The main advantage of this coupled model is its simplicity, as all those mechanisms were considered in a 1D FEM formulation.

## 2 A BRIEF REVIEW OF FEM FORMULATION

The Principle of Virtual Works postulates that the work done by internal forces on a virtual displacement field must be the same work done by the external forces acting on the structure. Based on Galerkin's method, the interpolation function can be expressed by the displacement field of the real problem (Bathe [2], Clough and Penzien [7], Felippa [12]):

$$\int_{\Omega} \{\varepsilon\}^T [D] \{\varepsilon\} d\Omega = \int_{\Omega} \{u\}^T \{b\} d\Omega \tag{1}$$

in which $\{\varepsilon\}$ is the actual strain field from the actual displacement field $\{u\}$, $[D]$ represents the fourth-order tensor elastic materials properties and $\Omega$ is the structure domain.

The FEM solves the problem dividing it into a finite number of subsets $\Omega_j$, called finite elements. The equation system is then represented by the sum of the contributions of each finite element, as:

$$\sum_{j=1}^{n}\left[\int_{\Omega_j}\{\varepsilon\}^T[D]\{\varepsilon\}d\Omega\right]=\sum_{j=1}^{n}\left[\int_{\Omega_j}\{u\}^T\{b\}d\Omega\right] \tag{2}$$

Fields $\{u\}$ and $\{\varepsilon\}$ are defined by the product of interpolation functions and nodal parameters of the finite elements, as:

$$\begin{aligned}\{u\}&=[H]\{u_j\}\\ \{\varepsilon\}&=[B]\{u_j\}\end{aligned} \tag{3}$$

in which $[H]$ and $[B]$ are, respectively, the known interpolation functions matrices for the displacement and strain and $\{u_j\}$ is the vector of the nodal displacements of each finite element. Placing Eq. (3) in (2) results in:

$$\sum_{j=1}^{n}\left[\{u_j\}^T\left(\int_{\Omega_j}[B]^T[D][B]d\Omega\right)\{u_j\}\right]=\sum_{j=1}^{n}\left[\{u_j\}^T\int_{\Omega_j}[H]^T\{b\}d\Omega\right] \tag{4}$$

Equation 4 represents the total energy potential of the solid defined by the contribution of all finite elements. The classical equation system of the FEM can be reached by the minimization of this total energy potential. Therefore, the process is defined by:

$$\sum_{j=1}^{n}\left(\left[K_j\right]\{u_j\}\right)=\sum_{j=1}^{n}\left(\{F_j\}\right) \tag{5}$$

in which $\left[K_j\right]=\int_{\Omega_j}[B]^T[D][B]d\Omega$ and $\{F_j\}=\int_{\Omega_j}[H]^T\{b\}d\Omega$. For nonlinear problems, the stiffness matrix $[K]$ depends on the actual displacements intensity and Eq. (5) must be expressed as:

$$\sum_{j=1}^{n}\left(\left[K_j(u_j)\right]\{u_j\}\right)=\sum_{j=1}^{n}\left(\{F_j\}\right) \tag{6}$$

## 3 NONLINEARITY OF THE MATERIALS

### 3.1 Damage model for concrete

The nonlinear behavior of the concrete originates from the crack growing along the concrete mass. Damage models are particularly interesting, because they allow penalizing the material stiffness in

function of the strain increase. In this study, we adopted the Mazars' damage model [24], which is grounded in the following hypotheses: damage is an isotropic variable, the residual strains are totally neglected, as depicted in Fig. 1 and damage occurs by tensile strains.

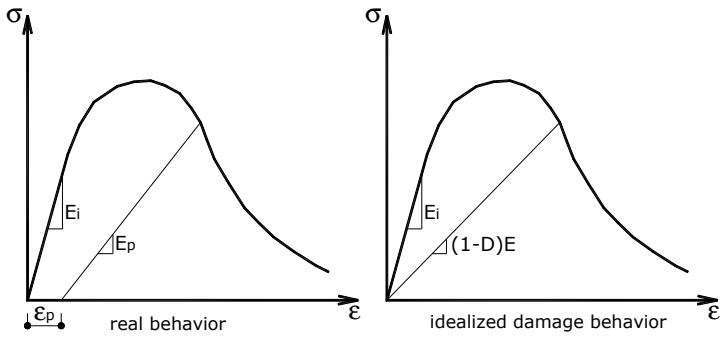


Figure 1 Real and idealized concrete behavior

The state of stretching at a point can be represented by the equivalent strain as:

$$\tilde{\varepsilon} = \sqrt{\left(\varepsilon_1\right)_+^{\,2} + \left(\varepsilon_2\right)_+^{\,2} + \left(\varepsilon_3\right)_+^{\,2}} \tag{7}$$

in which $\left(\varepsilon_i\right)_+$ corresponds to the positive components of the main strain tensor. Thus, one has $\left(\varepsilon_i\right)_+ = \left[\varepsilon_i + \left|\varepsilon_i\right|\right]/2$, with $\left(\varepsilon_i\right)_+ = \varepsilon_i$ in case of $\varepsilon_i > 0$ or $\left(\varepsilon_i\right)_+ = 0$ in case of $\varepsilon_i < 0$.

The criterion to verify the material integrity at a point is given by:

$$f = \tilde{\varepsilon} - \hat{S}(D) < 0 \tag{8}$$

Function $\hat{S}(D)$ represents the limit strain value in function of the damage. At the beginning of the incremental-iterative process, $\hat{S}(D)$ receives the strain value corresponding to the concrete tensile strength $\varepsilon_{d0}$. In the following steps $\hat{S}(D)$ is updated by the $\tilde{\varepsilon}$ value of the last step with damage. Due to the non symmetry of the concrete behavior in tension and compression, the damage variable is formed by the sum of two independent parts: tensile portion $D_T$ and compression portion $D_C$. Each of these portions indicates tensile and compression contribution to the local strain state and can be obtained in function of the equivalent strain and the internal parameters of the damage model as:

$$D_T = 1 - \frac{\varepsilon_{d0}\left(1 - A_T\right)}{\tilde{\varepsilon}} - \frac{A_T}{e^{\left[B_T\left(\tilde{\varepsilon} - \varepsilon_{d0}\right)\right]}}$$
$$D_C = 1 - \frac{\varepsilon_{d0}\left(1 - A_C\right)}{\tilde{\varepsilon}} - \frac{A_C}{e^{\left[B_C\left(\tilde{\varepsilon} - \varepsilon_{d0}\right)\right]}} \tag{9}$$

in which $\varepsilon_{d0}$, $A_T$, $B_T$, $A_C$, $B_C$ are the internal parameters of Mazars' damage. Indices T and C refer to tension and compression, respectively.

After reaching each part of the damage, the final value of the point strain state is given by

$$D = \alpha_T D_T + \alpha_C D_C \tag{10}$$

Coefficients $\alpha_T$ and $\alpha_C$ can be calculated by:

$$\alpha_T = \frac{\sum_i \left(\varepsilon_{Ti}\right)_+}{\varepsilon_V^+} \quad \text{e} \quad \alpha_C = \frac{\sum_i \left(\varepsilon_{Ci}\right)_+}{\varepsilon_V^+} \tag{11}$$

in which $\varepsilon_{Ti}$ and $\varepsilon_{Ci}$ are calculated from the main stresses considering elastic material and $\varepsilon_V^+$ represents the total state of stretching given by $\varepsilon_V^+ = \sum_i \left(\varepsilon_{Ti}\right)_+ + \sum_i \left(\varepsilon_{Ci}\right)_+$.

After damage, the stress state at the point is defined by:

$$\sigma = \left(1 - D\right) E \varepsilon$$
$$\tau = \left(1 - D\right) G \gamma \tag{12}$$

in which $E$ and $G$ are, respectively, the longitudinal and transversal elasticity modules of the material and $\varepsilon$ and $\gamma$ are, respectively, the longitudinal and transversal strains.

### 3.2 Plasticity model for steel

Steel has an elastic behavior until it reaches the yield stress. After that, there are some movements in the internal crystals of the material, which give it a new strength capacity. In this phase, called hardening, there is loss of stiffness, but the material still presents strength capacity until it reaches its rupture limit. The models based on the plasticity theory are appropriate to describe such a behavior (Owen and Hinton [28]). Thus, the model chosen for the steel is defined by an elastoplastic constitutive law with positive isotropic hardening, as depicted in Fig. 2.

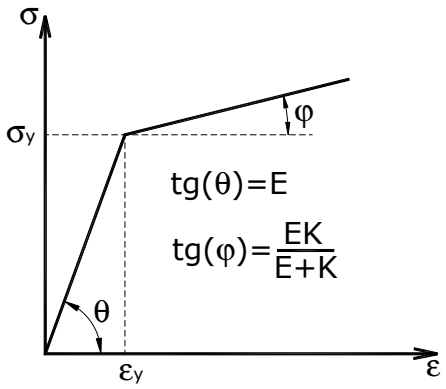


Figure 2 Elastoplastic steel behavior

The criterion to verify the elastoplastic steel behavior is given by:

$$f = \sigma_s - \left(\sigma_{sy} + K\alpha\right) < 0 \tag{13}$$

in which $\sigma_s$ is the steel reinforcement layer stress, $\sigma_{sy}$ is the steel yielding stress, $K$ is the hardening plastic modulus and $\alpha$ is an equivalent plastic strain measurement.

The stress over each reinforcement layer can be written as:

$$\begin{aligned} f \le 0 &\rightarrow \sigma = E\varepsilon \\ f > 0 &\rightarrow \sigma = E_t\varepsilon \end{aligned} \tag{14}$$

in which $E_t$ is the tangent elasticity modulus given by $E_t = EK/\left(E+K\right)$. It is interesting to note that the expression of the tangent elasticity modulus is valid only for monotonically crescent loading models.

## 4 GEOMETRIC NONLINEARITY

Fig. 3 illustrates the initial and final configurations of a point P in a solid after the loading action. The horizontal and vertical displacements are defined by:

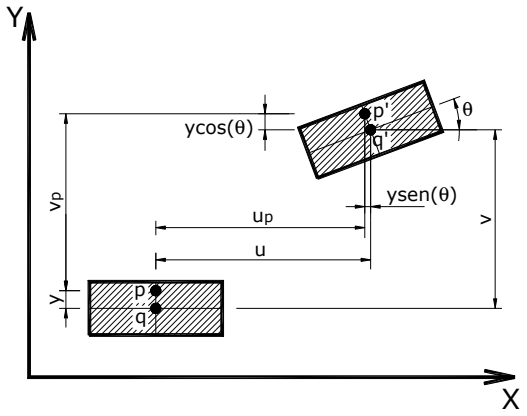


Figure 3 Initial and final configuration of a point

$$\begin{aligned} u_p(x,y) &= u(x) - y\sin(\theta) \\ v_p(x,y) &= v(x) - y + y\cos(\theta) \end{aligned} \tag{15}$$

Considering a second-order approximation for small displacements, where $\sin\theta = v'(x)$ and $\cos\theta = 1 - v'^2(x)/2$, one can write Eq. (15) as:

$$\begin{aligned} u_p(x,y) &= u(x) - yv'(x) \\ v_p(x,y) &= v(x) - y\frac{v'(x)^2}{2} \end{aligned} \tag{16}$$

in which $u$ and $v$ correspond, respectively, to the horizontal and vertical displacement fields of any point of the bar.

Considering the geometric nonlinearity second-order terms given by Green strain measurement, the longitudinal and transversal strain fields, $\varepsilon_{xx}$ and $\gamma_{xy}$, respectively, are written by:

$$\begin{aligned} \varepsilon_{xx} &= \frac{\partial u_p}{\partial x} + \frac{1}{2}\left[\left(\frac{\partial u_p}{\partial x}\right)^2 + \left(\frac{\partial v_p}{\partial x}\right)^2\right] \\ \gamma_{xy} &= \frac{\partial u_p}{\partial y} + \frac{\partial v_p}{\partial x} + \left(\frac{\partial u_p}{\partial x}\frac{\partial u_p}{\partial y} + \frac{\partial v_p}{\partial x}\frac{\partial v_p}{\partial y}\right) \end{aligned} \tag{17}$$

Eq. (16) and (17) provide the final expression for the strains field, which is written in function of the displacements for the frame finite element:

$$\begin{aligned}\varepsilon_{xx} &= u' + \frac{1}{2}(u')^2 + \frac{1}{2}(v')^2 - yv''(1+u') \\ \gamma_{xy} &= v' - \varphi - u'v' - \frac{v'^3}{2}\end{aligned} \tag{18}$$

in which $\varphi$ is the additional rotation term of Timoshenko's kinematics.

Green's strain tensor is naturally conjugated by the second Piola-Kirchhoff stress tensor. However, in the field of small displacements and strains, the second Piola-Kirchhoff stress tensor can be replaced by the conventional stress tensor (Paula [29]):

$$\underline{S} = \underline{\underline{D}}_0 \begin{Bmatrix} \varepsilon_{xx} \\ \gamma_{xy} \end{Bmatrix} \tag{19}$$

in which $\underline{S}$ is the conventional stress tensor with longitudinal and transversal component and $\underline{\underline{D}}_0$ is the material's elastic properties tensor written as $\underline{\underline{D}}_0 = \begin{bmatrix} E & 0 \\ 0 & G \end{bmatrix}$.

The updated lagrangian formulation describes the structure situation based on the last balanced configuration. Thus, all the information necessary for the next load step is taken from the last converged step. In practical terms, this idea means two updates: positions in each node of the structure and stresses in each integration point along the finite element. The stress tensor is updated by relating Cauchy's tensor with the second Piola-Kirchhoff stress tensor. However, for small displacements and strains, Cauchy's tensor in the current configuration coincides with the second Piola-Kirchhoff tensor of the last configuration. Thus, the update occurs simply by adding the extra stress of the current step to the last step values, as follows:

$$\begin{aligned} x &= x_a + \Delta x \\ y &= y_a + \Delta y \end{aligned} \tag{20}$$

$$\begin{aligned} \sigma_{xx} &= \sigma_{xx_a} + \Delta\sigma_{xx} \\ \tau_{xy} &= \tau_{xy_a} + \Delta\tau_{xy} \end{aligned} \tag{21}$$

in which $x_a$ and $y_a$ are the nodes positions in the $x$ and $y$ directions of the last step, $\Delta x$ and $\Delta y$ are the displacements of the current step, $\sigma_{xx_a}$ and $\tau_{xy_a}$ are the axial and tangential stresses of the last step and $\Delta\sigma_{xx}$ and $\Delta\tau_{xy}$ are the extra stresses calculated in the current step.

## 5 SHEAR STRENGTH MODEL

Fig. 4 shows a portion of a cracked reinforced concrete member with the shear force from each stress transfer mechanism.

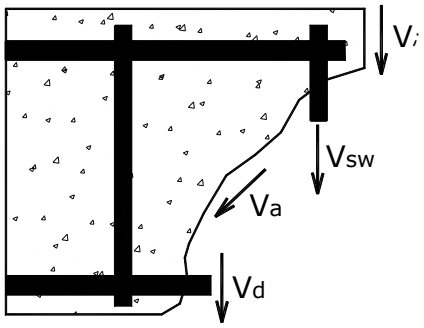


Figure 4 Cracked reinforced concrete member and shear force portions

The concrete contribution, $V_c$, is given by the $V_i$ and $V_a$ portions, which are related to the intact concrete and the aggregate interlock, respectively. The contributions of the longitudinal and transversal reinforcements are given by the dowel action $V_d$ and shear reinforcement $V_{sw}$, respectively.

### 5.1 Intact concrete and aggregate interlock contributions

The contributions of the concrete are given according to the criterion:

$$\begin{aligned} &D = 0 \rightarrow V_c = V_i \\ &0 < D < 1 \rightarrow V_c = V_a \end{aligned} \tag{22}$$

One of the mostly used forms to take into account the aggregate interlock existence is reducing the transversal elasticity modulus by a factor that depends essentially on the diagonal opening cracks (Walraven [33], Millard and Johnson [25], He and Kwan [16], Martín-Perez and Pantazopoulou [23]). This opening crack measurement can be approximated by the main tensile strain $\varepsilon_1$. Therefore, the new value of $G$ is given by $\mu G$, where $\mu$ is a number between 0 and 1 that depends on $\varepsilon_1$. This paper proposes to consider this reduction in function of the material damage state. It is assumed that the calibration of the damage model internal parameters in function of the tensile and compression experimental results in the concrete specimens automatically considers this effect of the aggregate interlock. As the damage variable is a function of the main strain state at a point, strain $\varepsilon_1$ also influences directly the reduction in the concrete transversal stiffness. Thus, the intact concrete and the aggregate interlock strength portions are assessed by the integration of the shear stresses along the reinforced concrete finite elements cross-section as follows:

$$V_i = \int_{-h/2}^{h/2} G\gamma_{xy}\, dy$$
$$V_a = \int_{-h/2}^{h/2} (1-D) G\gamma_{xy}\, dy \tag{23}$$

in which $h$ is the cross-section height.

### 5.2 Dowel action contribution

The dowel action is a shear strength complementary mechanism attributed to the concrete. However, it occurs when cracks cut across the longitudinal reinforcement bars, providing an increase in the shear strength. The faces of the crack transfer shear stresses to reinforcement bars, which start a local bending and shear at the bars. The dowel action can significantly increase the shear strength, as well as the post-peak ductility of some structural elements, such as beams with few or no shear reinforcement. In this model, the reinforcement bars work as beams over the elastic foundation of the concrete. Therefore, the dowel action behavior may be affected by several factors, such as the bars position along the cross-section, concrete cover and longitudinal and transversal reinforcement ratio. Fig. 5 shows the development of the dowel forces in a reinforced concrete cracked member. The bending moment caused by the dowel action can be given by:

$$M_d = V_d L \tag{24}$$

in which $V_d$ is the dowel shear force and $L$ is the finite element length.

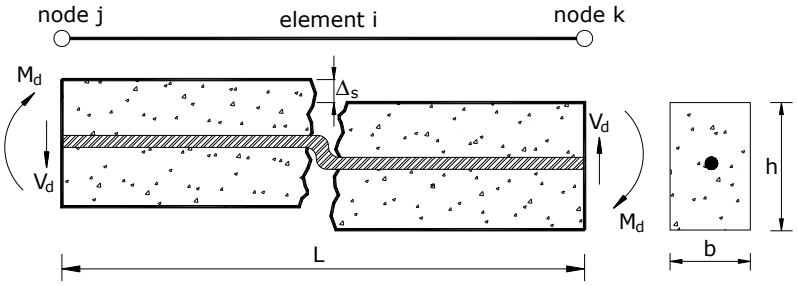


Figure 5 Dowel action mechanism along the cracked reinforced concrete member

The criterion for the beginning of the dowel action contribution is given by the same damage criterion. Fig. 6 presents the proposed criterion to initiate the dowel action contribution. The existence of damage is verified in the integration points immediately before and after the reinforcement layer. If the two points are damaged, that reinforcement layer will contribute to the dowel action.

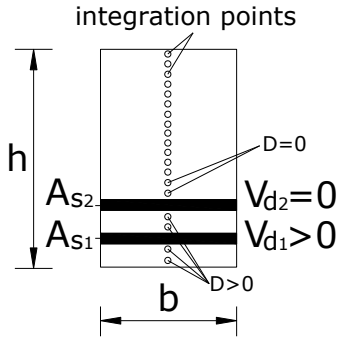


Figure 6 Criterion for dowel action existence along the cross-section

He and Kwan [16] proposed an interesting formulation to estimate both the dowel force and the dowel displacement:

$$V_d = E_s I_s \lambda^3 \Delta_s \leq V_{du} \tag{25}$$

The parameters involved in the $V_d$ calculations are:

$$I_s = \frac{\pi \varphi_s^4}{64},\ \lambda = \sqrt[4]{\frac{k_c \varphi_s}{4 E_s I_s}},\ k_c = \frac{127 c \sqrt{f_c}}{\sqrt[3]{\varphi_s^2}} \tag{26}$$

in which $E_s$ is the steel elasticity modulus, $I_s$ is the moment of inertia of a circular cross-section bar, $\varphi_s$ is the bar diameter, $\lambda$ is a parameter that compares the surrounded concrete stiffness with the bars stiffness, $\Delta_s$ is the dowel displacement, $k_c$ represents the stiffness coefficient of the surrounding concrete, $f_c$ is the concrete compression strength and $c$ is an experimental parameter that reflects the spacing between the bars. Values between 0.6 and 1.0 may be assumed. In this paper 0.8 was adopted for parameter $c$.

The dowel strength is limited by the ultimate shear capacity of the bar, which is given by:

$$V_{du} = 1.27 \varphi_s^2 \sqrt{f_c} \sqrt{\sigma_{sy}} \tag{27}$$

Diameter $\varphi_s$ of the bars is replaced by an equivalent diameter $\varphi_{s,eq}$ calculated in function of the reinforcement area of each layer, as:

$$\varphi_{s,eq} = \sqrt{\frac{4 A_s}{\pi}} \tag{28}$$

$$V_d = \frac{2\sqrt{\pi A_s}}{\pi} E_s I_s \lambda^3 \Delta_s \leq V_{du} \tag{29}$$

The dowel displacement of the cross-section of a finite element can be approximated by the arithmetic mean of the values assessed for each integration point (He and Kwan [16]), as:

$$\Delta_s = \frac{\sum_{i=1}^{n_{ht}} \left\{ \frac{\pi}{\lambda} \left[ \varepsilon_1 \cos(\alpha) \sin(\alpha) + \gamma_{xy} \cos^2(\alpha) \right] \right\}_i}{n_{ht}} \tag{30}$$

in which $\alpha$ is the main tensile direction defined over the horizontal plane and $n_{ht}$ is the number of integration points along the cross-section of a finite element.

### 5.3 Shear reinforcement contribution

In traditional modelings with one-dimensional finite elements, the contribution of the transversal reinforcement is not considered. Therefore, it becomes necessary to introduce an approximated model to take into account its influence, especially when shear stresses cannot be neglected. In beams with high span-to-depth ratio, the bi-dimensional stress state causes an increase in the damage, which is assessed considering the shear and normal stresses. In these cases, the concrete quickly loses its stiffness and the presence of shear reinforcement becomes necessary to guarantee the loading capacity of the cross-sections. According to Belarbi and Hsu [4], shear reinforcement presents significant strains only after the beginning of the concrete diagonal cracking. Prior to such cracking, the stresses are resisted by both the intact concrete over the non-damaged region and the aggregate interlock mechanism over the regions of low levels of damage. For the concrete, the diagonal cracks opening is directly associated with the main tensile strain $\varepsilon_1$. In the same way, the damage model criterion is based on the presence of tension in the main strain tensor, which allows admitting that the stirrups will be loaded after the beginning of the damaging of the concrete. Thus, the criterion to initiate the shear reinforcement contribution along the loading process is given by the same damage criterion, as expressed in equation 8. The main idea of the model consists in transferring part of the shear force dissipated by the damaging effect to the stirrups, as depicted in Fig. 7. While the equivalent strain does not reach the limit imposed by the damage criterion, the shear force in the stirrups is zero. After reaching this limit, the total strain can be separated into two parts:

$$\varepsilon = \varepsilon_e + \varepsilon_d \tag{31}$$

in which $e$ represents the elastic strain portion and $d$ is the dissipated portion.

From Eq. (12) one can write the dissipated strain portion as $\varepsilon_d = D\varepsilon$. In the same way, the damaged stress portion is written by $\sigma_d = DE\varepsilon$.

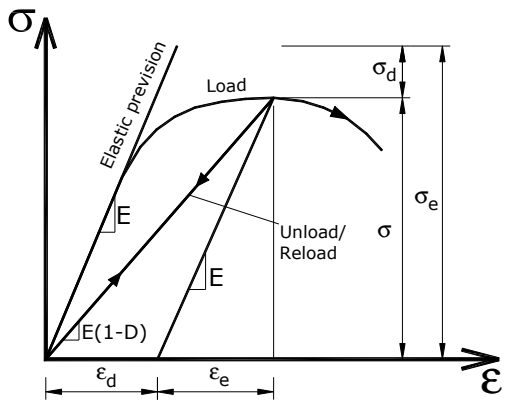


Figure 7 Scheme for stress transfer from concrete to stirrups

The Ritter-Mörsch's truss analogy was used to calculate the stirrups transferred force portion. Sanches Jr and Venturini [30] considered the stress state of the middle point to define the stirrups strain. However, in nonlinear behavior the stirrup stresses increase from the compressed flange toward the tensioned flange, but decrease in the regions close to the longitudinal tensile reinforcement. Points localized between the cross-section central line and the closest reinforcement layer must be verified because their strains may be larger than those obtained in the cross-section middle point. To describe the equilibrium, the cross-section point with the largest strain was adopted and assessed by the maximum value of the rotated main strain damaged portion toward the reinforcement direction. Mathematically, one has:

$$\varepsilon_{sw} = \max\left[\varepsilon_1 D \sin(\alpha)\right] \tag{32}$$

in which $\varepsilon_{sw}$ is the stirrups strain, $\alpha$ is the main tensile direction, as depicted in Fig. 8, and *max* represents the maximum operator.

The resultant shear force in each stirrup can be assessed by $\sigma_{sw} A_{sw}$, where $A_{sw}$ corresponds to a single stirrup cross-section area and $\sigma_{sw}$ is the stirrup stress. This stress value is obtained by the elastoplastic model over strain $\varepsilon_{sw}$. According to the Ritter-Mörsch's truss analogy, the shear force resisted by the stirrups can be calculated for a range of width equal to the effective depth of section $d$. Therefore, the shear reinforcement contribution can be written as:

$$V_{sw} = \sigma_{sw} \rho_{sw} b d \tag{33}$$

in which $\rho_{sw}$ is the transversal reinforcement ratio defined by $A_{sw}/(sb)$, $s$ is the spacing between the stirrups and $b$ is the cross-section width.

## 6 SOLUTION OF THE NONLINEAR PROBLEM

The Newton-Raphson's technique with tangent matrix was used to solve the nonlinear problem. The loading process is transformed into an incremental-iterative process, in which the stiffness matrix is constructed by the contribution of each integration point. Thus, the integrals expressed by Eq. (6) are converted into a discrete sum of all the material's contributions.

The stiffness matrix of each finite element $[K]$ is composed of three parts: concrete bending $[K]_{c,flex}$, concrete shear $[K]_{c,cis}$ and longitudinal reinforcement $[K]_s$:

$$[K]=[K]_{c,flex}+[K]_{c,cis}+[K]_s \tag{34}$$

$$\begin{aligned}
[K]_{c,flex} &= \sum_{i=1}^{nl}\left\{\sum_{j=1}^{nh}\left[B_{xx,ij}^T\left(1-D_{ij}\right)E_cB_{xx,ij}+B_{xx,ij}^T\eta_{ij}E_cB_{xx,ij}+G_{xx,ij}S_{xx,ij}\right]\frac{bh}{2}w_{y,j}\right\}\frac{L}{2}w_{x,i}\\
[K]_{c,cis} &= \sum_{i=1}^{nl}\left\{\sum_{j=1}^{nh}\left[B_{xy,ij}^T\left(1-D_{ij}\right)G_cB_{xy,ij}+B_{xy,ij}^T\eta_{ij}G_cB_{xy,ij}+G_{xy,ij}S_{xy,ij}\right]\frac{bh}{2}w_{y,j}\right\}\frac{L}{2}w_{x,i}\\
[K]_s &= \sum_{i=1}^{nl}\left\{\sum_{j=1}^{ca}\left[B_{xx,ij}^TE_sB_{xx,ij}+G_{xx,ij}\sigma_{s,ij}\right]A_{s,j}\right\}\frac{L}{2}w_{x,i}
\end{aligned} \tag{35}$$

The internal forces in each finite element, i.e., normal forces $N$, shear forces $V$ and bending moments $M$ are obtained by:

$$N=N_c+N_s \tag{36}$$

$$V=V_l+V_a+V_d+V_{sw} \tag{37}$$

$$M=M_c+M_s+M_d \tag{38}$$

with:

$$N_c=\sum_{i=1}^{nl}\left\{\sum_{j=1}^{nh}\left[B_{xx,ij}^T\left(1-D_{ij}\right)E_c\varepsilon_{xx,ij}\right]\frac{bh}{2}w_{y,j}\right\}\frac{L}{2}w_{x,i}\ ;\ N_s=\sum_{i=1}^{nl}\left\{\sum_{k=1}^{ca}B_{xx,ik}^T\sigma_{s,ik}A_{s,i}\right\}\frac{L}{2}w_{x,i}\ ;$$

$$V_l+V_a=\sum_{i=1}^{nl}\left\{\sum_{j=1}^{nh}\left[B_{xy,ij}^T\left(1-D_{ij}\right)G_c\gamma_{xy,ij}\right]\frac{bh}{2}w_{y,j}\right\}\frac{L}{2}w_{x,i}\ ;\ V_d=\frac{2\sqrt{\pi A_{st}}}{\pi}E_sI_s\lambda^3\Delta_s\ ;\ V_{sw}=\sigma_{sw}\rho_{sw}bd\ ;$$

$$M_c=\sum_{i=1}^{nl}\left\{\sum_{j=1}^{nh}\left[B_{xx,ij}^T\left(1-D_{ij}\right)E_c\varepsilon_{xx,ij}y_j\right]\frac{bh}{2}w_{y,j}\right\}\frac{L}{2}w_{x,i}\ ;M_s=\sum_{i=1}^{nl}\left\{\sum_{k=1}^{ca}B_{xx,ik}^T\sigma_{s,ik}A_{s,i}y_{s,k}\right\}\frac{L}{2}w_{x,i}\ ;$$

$$M_d=\frac{2\sqrt{\pi A_{st}}}{\pi}E_sI_s\lambda^3\Delta_sL\ .$$

in which $nl$ and $nh$ are, respectively, the number of integration points along the length and height of each finite element, $ca$ is the number of longitudinal reinforcement layers in each finite element, $E_c$ and $G_c$ are, respectively, the longitudinal and transversal elasticity modules of the concrete, $b$, $h$ and $L$ are, respectively, the width, height and length of each finite element, $y$ and $y_s$ are, respectively, the distances of each integration point and each reinforcement layer until the middle point of the cross-section, $A_s$ is the area of each longitudinal reinforcement layer, $A_{st}$ is the sum of all the areas of the longitudinal reinforcement layers which contribute to the dowel action and $w_x$ and $w_y$ are, respectively, the weight-factors of each integration point on the length and height of the finite elements, $B_{xx}$ and $B_{xy}$ are the incidence matrices containing the derivatives of the finite elements shape functions, $G_{xx}$ and $G_{xy}$ are the incidence matrices of the geometric nonlinearity.

$$\begin{aligned} B_{xx} &= A^T + \left(A^T u\right)A^T + \left(B^T u\right)B^T - yC^T - y\left(C^T u\right)A^T - y\left(A^T u\right)C^T \\ B_{xy} &= D^T - \left(B^T u\right)A^T - \left(A^T u\right)B^T - \frac{3}{2}\left(B^T u\right)B^T\left(B^T u\right) \\ G_{xy} &= AA^T + BB^T - yAC^T - yCA^T \\ G_{xy} &= -BA^T - AB^T - 3\left(B^T u\right)BB^T \end{aligned} \tag{39}$$

The strain fields are related to the nodal parameters of the finite elements through the $A^T$, $B^T$, $C^T$, $D^T$ vectors, as:

$$\begin{aligned} A^T &= \begin{bmatrix} N_1^{'} & 0 & 0 & N_4^{'} & 0 & 0 \end{bmatrix} \\ B^T &= \begin{bmatrix} 0 & N_2^{'} & N_3^{'} & 0 & N_5^{'} & N_6^{'} \end{bmatrix} \\ C^T &= \begin{bmatrix} 0 & N_2^{''} & N_3^{''} & 0 & N_5^{''} & N_6^{''} \end{bmatrix} \\ D^T &= \begin{bmatrix} 0 & \dfrac{-2g}{(1+2g)L} & \dfrac{-g}{(1+2g)} & 0 & \dfrac{2g}{(1+2g)L} & \dfrac{-g}{(1+2g)} \end{bmatrix} \end{aligned} \tag{40}$$

in which $N_i^{'}$ and $N_i^{''}$ with $i = 1$ to 6 are first and second derivatives of the shape functions and $g$ is the Weaver's constant, which is $g = 6EI/0.833GAL$ for the rectangular cross-sections.

The shape functions of the problem are given by:

$$N_1 = \left(1 - \frac{x}{L}\right); N_2 = \left[1 - 3\left(\frac{x}{L}\right)^2 + 2\left(\frac{x}{L}\right)^3\right]; N_3 = L\left[\left(\frac{x}{L}\right) - 2\left(\frac{x}{L}\right)^2 + \left(\frac{x}{L}\right)^3\right]$$
$$N_4 = \left(\frac{x}{L}\right); N_5 = \left[3\left(\frac{x}{L}\right)^2 - 2\left(\frac{x}{L}\right)^3\right]; N_6 = L\left[-\left(\frac{x}{L}\right)^2 + \left(\frac{x}{L}\right)^3\right] \tag{41}$$

in which $x$ corresponds to any horizontal coordinate along the finite element length.

The $\eta$ function considers the equivalent strain derivatives related to the strain components and is assessed by:

$$\eta = F(\tilde{\varepsilon})\frac{\partial \tilde{\varepsilon}}{\partial \varepsilon} \tag{42}$$

According to Mazars' damage model, $F(\tilde{\varepsilon})$ is a linear combination of the tensile and compression damaging functions obtained with $F(\tilde{\varepsilon}) = \alpha_T F_T(\tilde{\varepsilon}) + \alpha_C F_C(\tilde{\varepsilon})$.

$$F_T(\tilde{\varepsilon}) = \frac{\varepsilon_{d0}(1 - A_T)}{\tilde{\varepsilon}^2} + \frac{A_T B_T}{e^{\left[B_T(\tilde{\varepsilon} - \varepsilon_{d0})\right]}}$$
$$F_C(\tilde{\varepsilon}) = \frac{\varepsilon_{d0}(1 - A_C)}{\tilde{\varepsilon}^2} + \frac{A_C B_C}{e^{\left[B_C(\tilde{\varepsilon} - \varepsilon_{d0})\right]}} \tag{43}$$

The derivative of the equivalent strain related to the horizontal portion of the strain tensor depends on the directions of the fiber strains according to:

$$\frac{\partial \tilde{\varepsilon}}{\partial \varepsilon_x} = 1 \text{ (tension) ou } \frac{\partial \tilde{\varepsilon}}{\partial \varepsilon_x} = -\nu\sqrt{2} \text{ (compression)} \tag{44}$$

A complete flowchart for the entire proposed FEM model is illustrated in Fig. 8. The boxes with a numerical index are explained in details because they describe the most important parts of the program, including all the developed particular models.

1 – Initial Data: in this section, one can check the models which will be considered in the numerical analysis, such as dowel action, shear reinforcement contribution, Euler-Bernoulli or Timoshenko's theory and the finite element mesh description;

2 – Starting Incremental Process: in this section, the program applies the load or displacement increment on the particular nodes of the mesh;

3 – Starting Iterative Process: in this section, the program starts the iterative process preparing all the internal variables of the damage and plasticity models, as well as the shear strength mechanisms;

4 – Local Stiffness Matrix: in this section, the stiffness matrix of each finite element is calculated, considering local degradation state and local plasticization state of the integration Gauss points on the cross-section and longitudinal reinforcement layers along the finite elements, respectively. The local stiffness matrix is evaluated by Eq. 34, in which the separated parts for concrete (bending and shear) and for longitudinal reinforcements steel are given by $[K]_{c,flex}$, $[K]_{c,cis}$ and $[K]_s$, respectively (evaluated by Eq. 35). Each of the variables used in these equations was already described, depending of the adopted shape functions and their derivatives, mechanical properties of the materials, geometry of the structure and internal variables of the damage and plasticity models (as described by Eq. 39 to 44).

5 – Internal Forces Assessment: in this section, the internal resistances forces are assessed taking into account material behaviors and shear complementary mechanisms, which are aggregate interlock and dowel action, as well as the contribution of shear reinforcement. The internal forces given by the normal force, shear force and bending moment in each cross-section over all the discretization points along the finite element length are assessed by Eq. (36), (37) and (38), respectively. It is necessary to identify each component of these calculations: $N_c$ and $N_s$ are the contributions of undamaged concrete and longitudinal reinforcement for normal forces; $V_l$ and $V_a$ are the contributions of undamaged concrete and aggregate interlock, respectively; $V_d$ and $V_{sw}$ are the contributions of the dowel action and shear reinforcement assessed by the developed models, respectively; $M_c$, $M_s$ and $M_d$ are the contributions of concrete, longitudinal reinforcement and the bending moment from dowel action, respectively.

The last parts of the program as depicted in Fig. 8 are classical in all the nonlinear numerical FEM models.

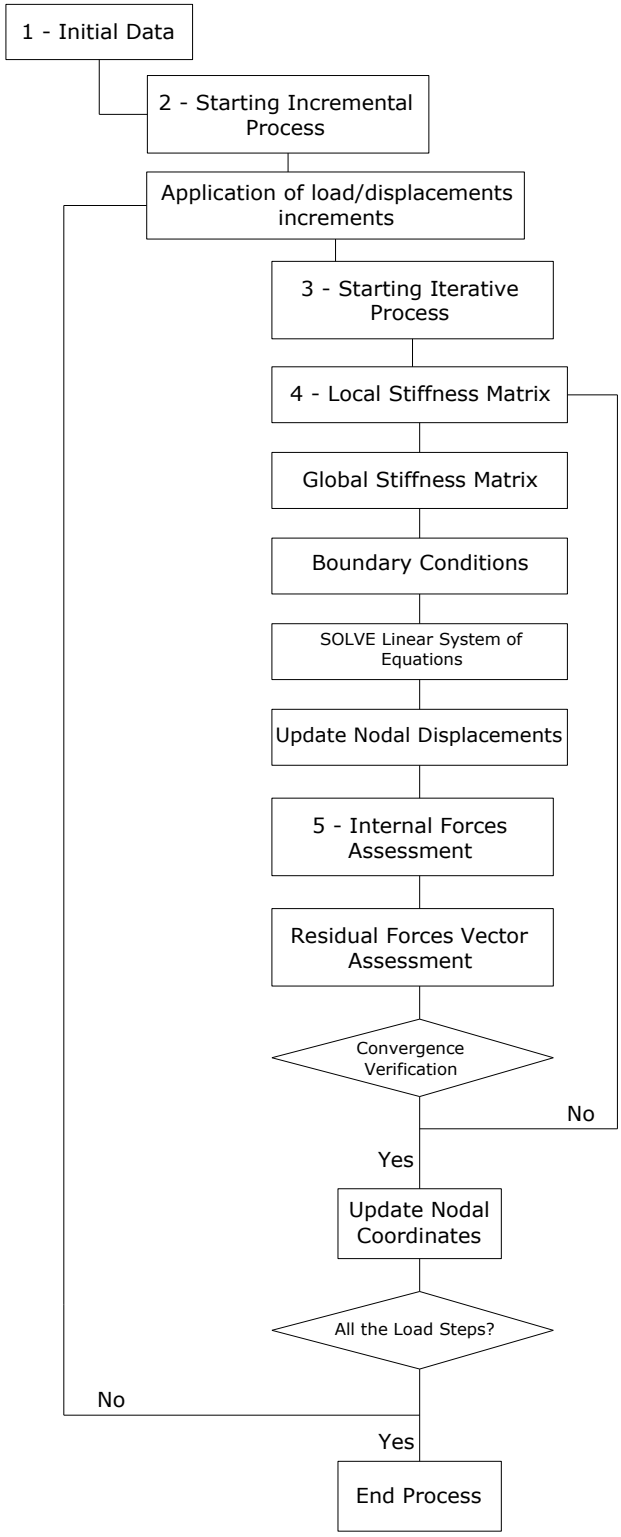


Figure 8 Flowchart of the developed FEM model

## 7 NUMERICAL APPLICATIONS

The common information to all the numeric examples is: force and displacement convergence tolerance to verify the equilibrium is $10^{-4}$; 6 and 20 integration points along the length and the cross-section of the finite elements, respectively. Value of the $K_S$ parameter for the elastoplastic behavior of the steel reinforcements is, in both examples, 10% of $E_S$.

### 7.1 Example 1

In this example three reinforced concrete beams with same geometry and loading, but different longitudinal and transversal reinforcement ratios were analyzed. The beams were experimentally tested by Ashour [1] and numerically tested by He and Kwan [16]. They considered the steel bars embedded in a quadrilateral isoparametric finite element (plain stress state) of concrete with two extra degrees of freedom for bending to eliminate the shear locking. The ultimate loads were compared with the results of Wang and Hoogenboom [34], who simulated beams from a stringer-panel bi-dimensional mechanical model, in which the cracked concrete was considered an orthotropic material. The reinforcement details, as well the mesh of 18 finite elements with different lengths are shown in Fig. 9. The mechanical parameters used for each beam are given in Table 1.

Table 1 Concrete and steel properties

| RC Beam | $f_c$ (MPa) | $E_c$ (MPa) | $\nu_c$ | $f_s$ (MPa) | $E_s$ (MPa) | $K_s$ (MPa) |
|---|---|---|---|---|---|---|
| 01 | 30.0 | 25921 | 0.24 | 500 | 205000 | 20500 |
| 02 | 33.1 | 27227 | 0.23 | 500 | 205000 | 20500 |
| 03 | 22.0 | 22198 | 0.26 | 500 | 205000 | 20500 |

The parameters of the damage model $\varepsilon_{d0}$, $A_T$, $B_T$, $A_C$ and $B_C$ were calibrated for each concrete compression strength and are given in Table 2. The mechanical models used in these analyses took into account the Timoshenko's theory only with the concrete contributions, i.e., intact concrete and aggregate interlock (T) and the full Timoshenko's theory with all the contributions (TSD).

The results of the analysis are depicted in Fig. 10, 11 and 12. It is possible to verify a considerable difference between the results of the T and TSD models in the two first beams, which shows the importance of the stress transfer from the cracked concrete to the shear reinforcement.

Table 2 Parameters of the damage model

| $f_c$ (MPa) | $\varepsilon_{d0}$ | $A_T$ | $B_T$ | $A_C$ | $B_C$ |
|---|---|---|---|---|---|
| 30.0 | 0.000078 | 1.004 | 9000 | 1.056 | 1034 |
| 33.1 | 0.000080 | 1.018 | 8997 | 1.048 | 963.3 |
| 22.0 | 0.000074 | 0.964 | 9011 | 1.081 | 1253 |

From the point of view of the equilibrium trajectory, the 1D FEM model considering TSD showed, for beam 01, a better behavior than that observed with the He and Kwan [12] 2D FEM model, as depicted in Fig. 10. The Mazars' damage model tends to produce better results for reinforced concrete members with higher reinforcement rates than for concrete members with lower reinforcement rates. Such a behavior is due to the damaging along the concrete member producing a better representation of the real cracking panorama. Moreover, the aggregate interlock defined by the damage model proved to be better considered in this case and also in the ultimate load and TSD was more accurate than the others, as seen in Table 3.

For beam 02, all the numerical modeling showed a more rigid behavior than the experimental results. The withdrawal of two reinforcement layers closer to the beam's geometric center and the largest vertical spacing between the layers demonstrated importance in the description of the equilibrium trajectory, but they did not provide a good agreement with the experimental results. However, in terms of ultimate load, the TSD model reached almost the same value obtained in the experimental test, as illustrated in Table 3.

Beam 03 presented almost the same result for the T and TSD models, since there was no shear reinforcement. The shear strength in this case was given by the intact concrete, aggregate interlock and dowel action portions. The dowel action influence was found to be small when compared to the shear transversal reinforcement. Therefore, the shear reinforcement together with the concrete contributions is responsible for the shear strength in deep reinforced concrete beams. The ultimate load value provided by the dowel action was different from the value observed in the T model (Table 3), indicating a small contribution to the final shear strength of the beam.

Table 3 Values of the ultimate load

| **Model** | **RC Beam** | $\mathbf{F_{ult}}$ **(kN)** | $\mathbf{F_{ult}}$ / $\mathbf{F_{exp}}$ |
|---|---|---|---|
| ***Experimental*** | *01* | ***1095.2*** | ***1.000*** |
| He and Kwan | | 1071.2 | 0.978 |
| Wang and Hoogenboom | | 1060.0 | 0.968 |
| This paper – T | | 701.8 | 0.641 |
| *This paper – TSD* | | *1090.8* | *0.996* |
| ***Experimental*** | *02* | ***947.6*** | ***1.000*** |
| He and Kwan | | 899.6 | 0.949 |
| Wang and Hoogenboom | | 814.0 | 0.859 |
| This paper – T | | 731.3 | 0.772 |
| *This paper – TSD* | | *953.9* | *1.007* |
| ***Experimental*** | *03* | ***567.6*** | ***1.000*** |
| He and Kwan | | 533.4 | 0.940 |
| Wang and Hoogenboom | | 456.0 | 0.803 |
| This paper – T | | 566.9 | 0.999 |
| *This paper – TSD* | | *567.8* | *1.000* |

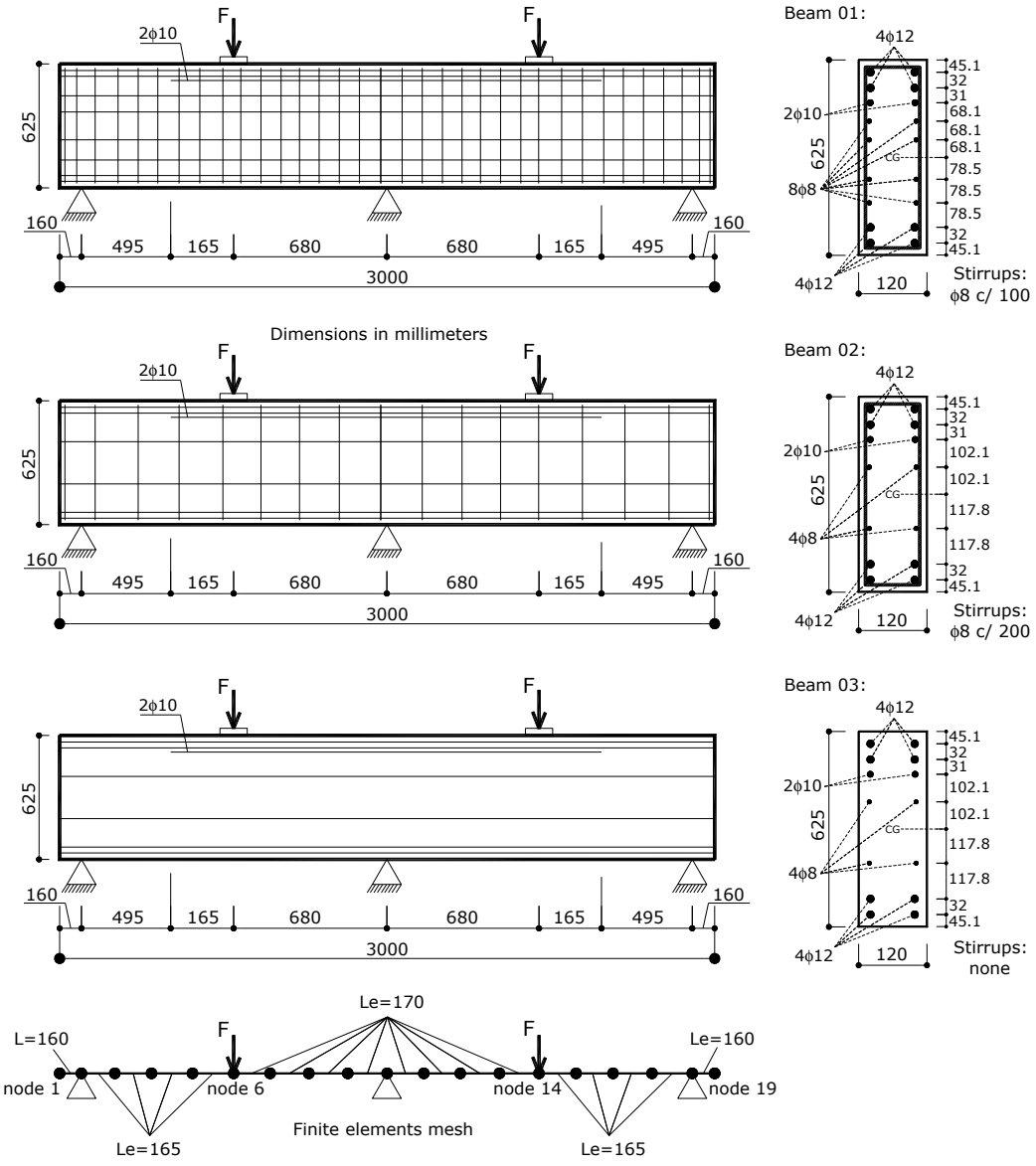


Figure 9 Geometry, loading and discretization of the analyzed beams

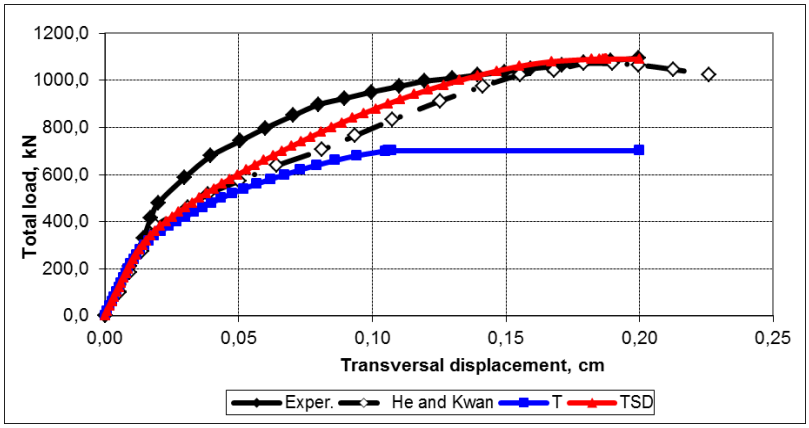


Figure 10 Equilibrium trajectory of vertical node 14: beam 01

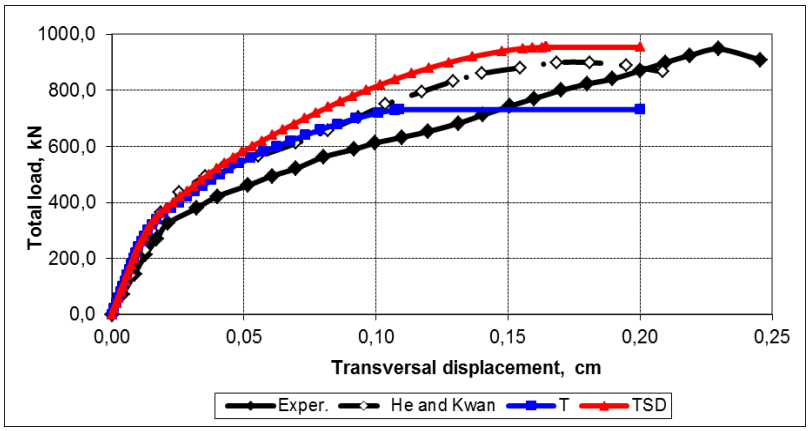


Figure 11 Equilibrium trajectory of vertical node 14: beam 02

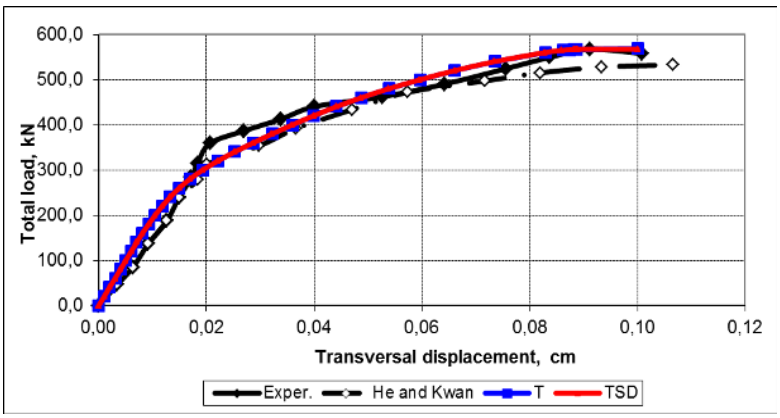


Figure 13 Equilibrium trajectory of vertical node 14: beam 03

## 7.2 Example 2

The structure studied in this example is a reinforced concrete frame tested by Vecchio and Emara [32] and numerically analyzed by Güner [15] and La Borderie et al. [20]. The considered models were Euler-Bernoulli (B) without shear contributions and full Timoshenko's (TSD). The loads and frame geometry are depicted in Fig. 13.

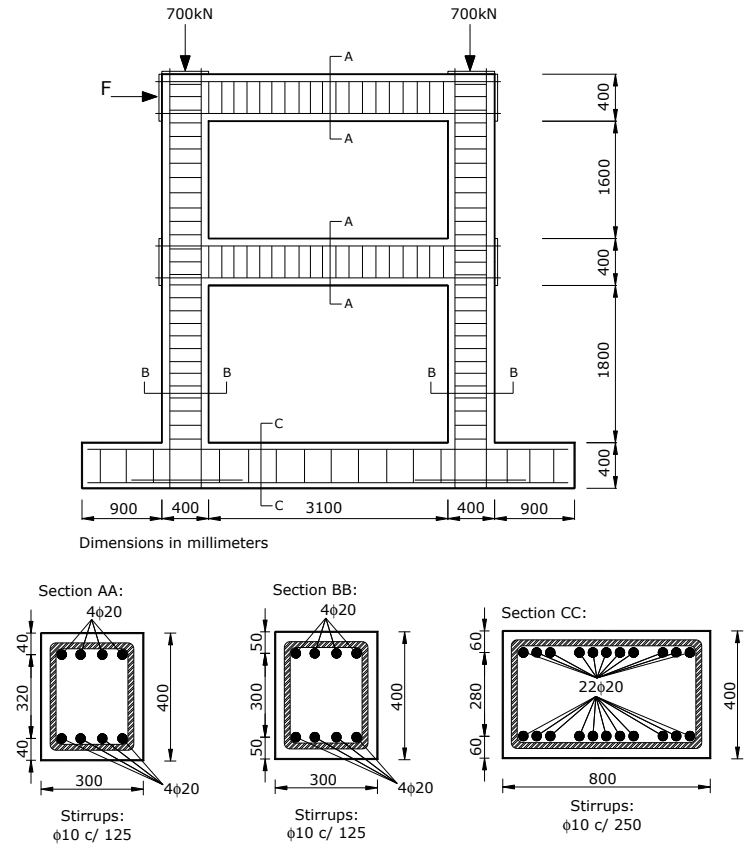


Figure 13 Geometry and loads of the reinforced concrete frame

Two types of support conditions were considered: case I – frame with a support beam and case II – clamped-clamped frame, as shown in Fig. 13. The response obtained by La Borderie et al. [20] was considered only for case II and repeated for case I. Concerning the types of analyses, Güner [15] used the SAP 2000 [8] software, in which the structure is considered with a mixed behavior, i.e., elastic-linear along the one-dimensional finite elements and plastic hinges at the appropriate member ends. These hinges are positioned at the end nodes of some special finite elements, such as the joint of a beam and column to simulate the existence of rigid offsets. The La Borderie et al. [20] modeling was performed with one-dimensional finite elements, but with their own damage model, in which the inelastic strains from the damage were taken into account.

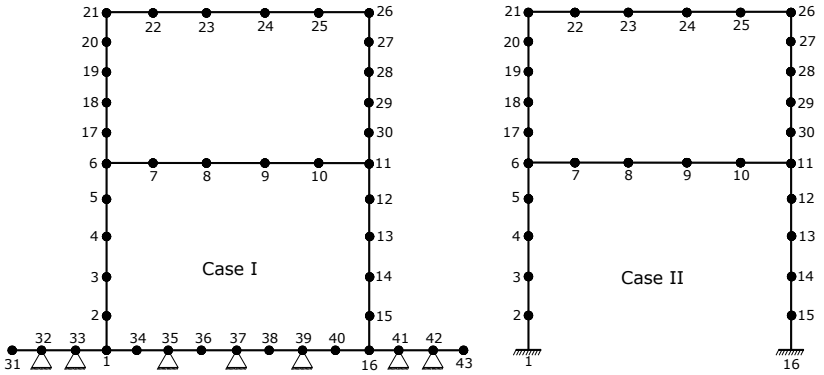


Figure 14 Cases of the support conditions considered

The parameters used were concrete elasticity modulus of 23674MPa, concrete compression strength of 30MPa, concrete Poisson's ratio of 0.2, steel yielding stress of 418MPa, steel elasticity modulus of 192500MPa and steel plastic modulus of 19250MPa. The horizontal loading on the frame top was applied in steps of 5kN. The damage parameters were, respectively, $\varepsilon_{d0}$, $A_T$, $B_T$, $A_C$, and $B_C$: 0.000085; 1.145; 10330; 1.117 and 1189. The equilibrium trajectories for cases I and II are depicted in Fig. 15 and 16.

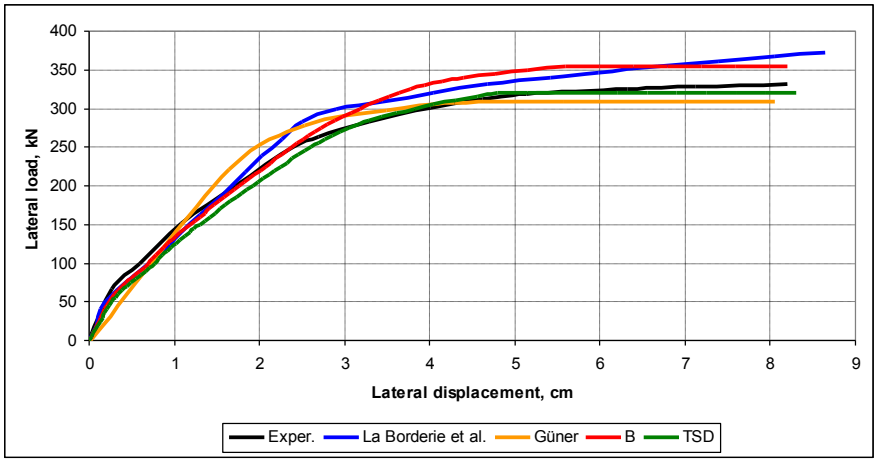


Figure 15 Horizontal equilibrium trajectory of node 21: case I

The use of clamped supports, as observed in case II, provided higher stiffness to the structure, since there was no rotation in the support nodes. The support beams adopted in case I did not show a significant difference for model B. However, for the TSD model, some changes were observed in terms of displacements after concrete cracking and especially in terms of ultimate load. The great capacity of internal forces redistribution may be the main reason for this behavior.

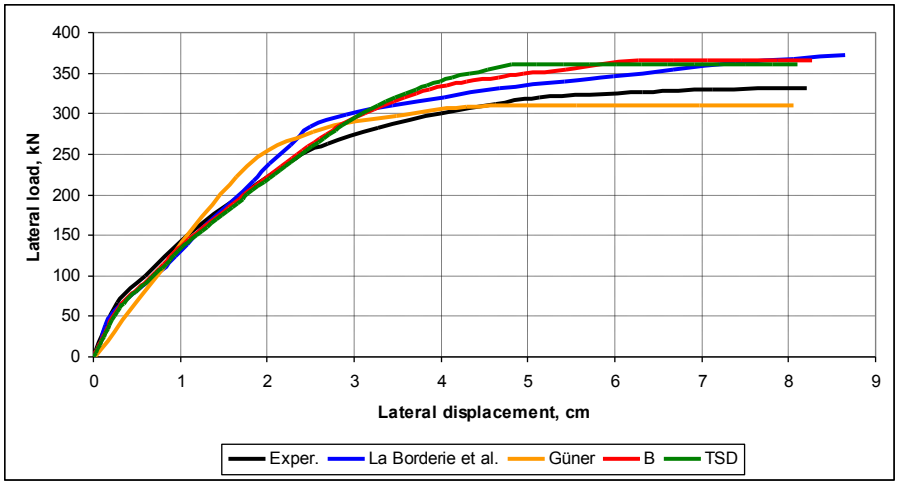


Figure 16 Horizontal equilibrium trajectory of node 21: case II

Tables 4 and 5 present the values of the loading and horizontal displacement for both reinforcement steel yielding in node 1 and frame ruin. The column Error (%) was evaluated from a comparison between experimental and each numerical result for both yielding and ultimate loads.

Table 4 Comparison between the results: case I

| **Model** | **Yielding** | | | **Ultimate** | | |
|---|---|---|---|---|---|---|
| | **F (kN)** | **d (cm)** | **Error (%)** | **F (kN)** | **d (cm)** | **Error (%)** |
| *Experimental* | *264.0* | *2.68* | *0.0* | *332.0* | *8.21* | *0.0* |
| Güner [15] with SAP2000 | 238.0 | 1.89 | -9.8 | 309.0 | 8.06 | -6.9 |
| La Borderie et al. [20] | 277.0 | 2.53 | +4.9 | 373.0 | 8.64 | +12.3 |
| B | 285.0 | 2.88 | +7.9 | 355.0 | 8.20 | +6.9 |
| *TSD* | *265.0* | *2.85* | *+0.4* | *320.0* | *8.31* | *-3.6* |

Table 5 Comparison between the results: case II

| **Model** | **Yielding** | | | **Ultimate** | | |
|---|---|---|---|---|---|---|
| | **F (kN)** | **d (cm)** | **Error (%)** | **F (kN)** | **d (cm)** | **Error (%)** |
| *Experimental* | *264.0* | *2.68* | *0.0* | *332.0* | *8.21* | *0.0* |
| Güner [15] with SAP2000 | 238.0 | 1.89 | -9.8 | 309.0 | 8.06 | -6.9 |
| La Borderie et al. [20] | 277.0 | 2.53 | +4.9 | 373.0 | 8.64 | +12.3 |
| B | 285.0 | 2.86 | +7.9 | 365.0 | 8.27 | +9.9 |
| *TSD* | *283.0* | *2.80* | *+7.2* | *360.0* | *8.10* | *+8.4* |

As one can observe, the TSD model for case I represented better the real behavior of the frame in terms of ultimate load and reinforcement steel yielding, showing differences of only -3.6% and +0.4%, respectively, in comparison to the experimental tests. In the case II, in which the structure is considered as a clamped-clamped frame, the proposed model was capable to obtain a good agreement compared to the other models regarding the experimental results, especially for the ultimate load.

## 8 CONCLUDING REMARKS

This paper presented a mechanical model based on the one-dimensional finite element method which incorporates the shear reinforcement strength, the dowel action and the aggregate interlock from the concepts of the damage mechanics, besides the geometric nonlinearity. One of its advantages consists in adapting the shear strength mechanisms for a bar finite element without 2D analysis. The results allowed concluding that the model could satisfactorily represent a structural behavior in which the influence of the shear strains must be considered, highlighting the contributions of the shear reinforcement, dowel action and aggregate interlock. The aggregate interlock portion was assessed together with the intact concrete portion given by the damage model. Thus, by calibrating the damage parameters, the aggregate interlock was automatically taken into account, because these parameters are obtained from the experimental tests of the concrete. The coupling between the shear strength complementary mechanisms, the damage model for concrete and geometric nonlinearity is also another interesting aspect. It allowed simulating frame structures, which take the equilibrium in the deformed configuration with the stiffness loss from bending and shear strain states. Finally, the model has showed numerical stability and capability of assessing the ultimate loads, the start of concrete cracking and the reinforcement steel yielding values of the analyzed structures with good accuracy.

**Acknowledgements** The authors would like to acknowledge FAPESP (São Paulo Research Foundation) for the financial support given to this project. A special "thanks" to professor W. S. Venturini (*in memoriam*).

## References

[1] ASHOUR, A.F. Tests of reinforced concrete continuous beams. ACI Structural Journal, v.97, n.1, p.3-12; 1997.

[2] BATHE, J.K. Finite element procedures in engineering analysis. Prentice-Hall, Englewood Cliffs; 1982.

[3] BAZANT, Z.P.; GAMBAROVA, P.G. Rough cracks in reinforced concrete. Journal of the Structural Division, ASCE, v.106, n.4, April, p.819-842; 1980.

[4] BELARBI, A.; HSU, T.T.C. Stirrup stresses in reinforced concrete beams. ACI Structural Journal, September-October, p.530-538; 1990.

[5] BELLETTI, B.; CERIONI, R.; IORI, I. Physical approach for reinforced-concrete (PARC) membrane elements. Journal of Structural Engineering, ASCE, v.127, n.12, December, p.1412-1426; 2001.

[6] BHATT, P.; KADER, M.A. Prediction of shear strength of reinforced concrete beams by nonlinear finite element analysis. Computers and Structures, v. 68, p. 139-155; 1998.

[7] CLOUGH, R.W.; PENZIEN, J. Dynamics of structures. 2nd Edition; 1993.

[8] CSI. Analysis reference manual for SAP2000®, ETABS® and SAFE™®. Computers and Structures, Inc., Berkeley, California, USA, 415 pp; 2005.

[9] DEI POLI, S.; DI PRISCO, M.; GAMBAROVA, P.G. Shear response, deformations and subgrade stiffness of a dowel bar embedded in concrete. ACI Structural Journal, v.89, n.6, November-December, p.665-675; 1992.

[10] DULACSKA, H. Dowel action of reinforcement crossing cracks in concrete. ACI Journal, Proceedings, v.69, n.12, December, p.754-757; 1972.

[11] EL-ARISS, B. Behavior of beams with dowel action. Engineering Structures, v.29, p.899-903; 2007.

[12] FELIPPA, C.A. Introduction to the finite element method – lecture notes. Boulder: University of Colorado; 2000.

[13] FRANTZESKAKIS, C.; THEILLOUT, J.N. Nonlinear finite element analysis of reinforced concrete structures with a particular strategy following the cracking process. Computers and Structures, v.31, n.3, p.395-412; 1989.

[14] GERGELY, P. Splitting cracks along the main reinforcement in concrete members. Dept. of Structural Engineering, Report, Cornell University, 1969.

[15] GÛNER, S. Performance assessment of shear-critical reinforced concrete plane frames. Toronto, PhD Thesis, University of Toronto, 429 p.; 2008.

[16] HE, X.G.; KWAN, K.H. Modelling dowel action of reinforcement bars for finite element analysis of concrete structures. Computers and Structures, v.79, p.595-604; 2001.

[17] INCE, R.; YALCIN, E.; ARSLAN, A. Size-dependent response of dowel action in R.C. members. Engineering Structures, n.29, p.955-961; 2007.

[18] JIMENES, R.; WRITE, R.N.; GERGELY, P. Bond and dowel capacities of reinforced concrete. ACI Journal, January, p.73-91; 1979.

[19] KREFELD, W.J.; THURSTON, C.W. Studies of the shear and diagonal tension strength of simply supported reinforced concrete beams. ACI Journal, v.63, n.4, p.451-476; 1966.

[20] LA BORDERIE, C.; MAZARS, J.; PIJAUDIER-CABOT, G. Response of plain and reinforced concrete structures under cyclic loadings. Cachan, France, Laboratoire de Mécanique et Technologie, Rapport Interne, n.123, 1991.

[21] LAIBLE, J.P.; WHITE, R.N.; GERGELY, P. Experimental investigation of seismic shear transfer across cracks in concrete nuclear containment vessels. Reinforced concrete structures in seismic zones. Detroit, American Concrete Institute, ACI Special Publication SP-53, p.203-206; 1977.

[22] MAITRA, S.R.; REDDY, K.S.; RAMACHANDRA, S. Load transfer characteristics of dowel bar system in joined concrete pavement. Journal of Transportation Engineering ASCE, v.135, n.11, November 1, p.813-821; 2009.

[23] MARTÍN-PEREZ, B.; PANTAZOPOULOU, S.J. Effect of bond, aggregate interlock, and dowel action on the shear strength degradation of reinforced concrete. Engineering Structures, v.23, p.214-227; 2001.

[24] MAZARS, J. Application de la mechanique de l'endommagement au comportement non lineaire et à la rupture du béton de structure, Paris, Thèse de Doctorat d'État, Université Paris 6; 1984.

[25] MILLARD, S.G.; JOHNSON, R.P. Shear transfer across cracks in reinforced concrete due to aggregate interlock and to dowel action. Magazine of Concrete Research, v.36, n.126, p.9-21; 1984.

[26] NOGUEIRA, C.G. Desenvolvimento de modelos mecânicos, de confiabilidade e de otimização para aplicação em estruturas de concreto armado. São Carlos, Tese (doutorado) - Escola de Engenharia de São Carlos, Universidade de São Paulo, 345 p.; 2010.

[27] OLIVER, J.; LINERO, D.L.; HUESPE, A.E.; MANZOLI, O.L. Two-dimensional modeling of material failure in reinforced concrete by means of a continuum strong discontinuity approach. Computer Methods in Applied Mechanics and Engineering, v.197, p.332-348; 2008.

[28] OWEN, D.R.J.; HILTON, H. Finite elements in plasticity. Swansea, U.K, Pineridge Press; 1980.

[29] PAULA, C.F. Contribuição ao estudo das respostas numéricas não-lineares estática e dinâmica de estruturas reticuladas planas. São Carlos, Tese (doutorado) - Escola de Engenharia de São Carlos, Universidade de São Paulo, 128 p.; 2001.

[30] SANCHES JR, F.; VENTURINI, W.S. Damage modelling of reinforced concrete beams. Advances in Engineering Software, v.38, p.538-546; 2007.

[31] SOLTANI, M.; AN, X.; MAEKAWA, K. Localized nonlinearity and size-dependent mechanics of in-plane RC element in shear. Engineering Structures, v.27, p.891-908; 2005.

[32] VECCHIO, F.J.; EMARA, M.B. Shear deformations in reinforced concrete frames. ACI Structural Journal, v.89, n.01, p.46-56; 1992.

[33] WANG, Q.; HOOGENBOOM, P.C.J. Nonlinear analysis of reinforced concrete continuous deep beams using stringer-panel model. Asian Journal of Civil Engineering (Building and Housing), v.5, n.1-2, p.25-40; 2004.

[34] WALRAVEN, J.C. Fundamental analysis of aggregate interlock. Journal of the Structural Division, ASCE, v.107, n.ST11, November, p.2245-2270; 1981.